JOURNAL OF MATERIALS SCIENCE 33 (1998) 3037–3045

Infiltration-processed, functionally graded aluminium titanate/zirconia–alumina composite

Part I *Microstructural characterization and physical properties*

S. PRATAPA*, I. M. LOW‡, B.H. O'CONNOR
Materials Research Group, Department of Applied Physics, Curtin University of Technology, GPO Box U1987, Perth WA 6845, Australia
E-mail: rlowim@cc.curtin.edu.au

A novel route for processing aluminium titanate (AT)/(alumina–zirconia (AZ)) with graded microstructure and properties is described. This process offers a simple means of tailoring the composition and microstructure of ceramic materials. The processing involves infiltrating porous AZ preforms with a solution of $TiCl_4$, followed by sintering at 1550 °C for 3 h. The resultant material has a homogeneous core encased with a graded and heterogeneous layer of AT/AZ. Analyses by X-ray diffraction and energy-dispersive spectrometry have revealed the existence of concentration gradients, the AT content decreasing with increasing sample depth. The presence of both AT and zirconia inhibits the growth of alumina grains through a pinning mechanism. The existence of microcracking in AT and zirconia grains has been revealed by scanning electron microscopy. The graded material displays gradual changes in thermal expansion values due to the presence of AT which gradually reduces in amount from the surface to the core. The inclusion of zirconia has a favourable effect on the thermal stability of AT against phase decomposition.

1. Introduction

Both alumina and aluminium titanate (AT) are ceramics showing considerable promise for use in a number of engineering applications. The former is widely used in areas where wear, chemical and/or heat resistance are required. Owing to its low thermal expansion, excellent thermal shock resistance and low thermal conductivity, the latter is a promising material for use as a refractory and also as a thermal insulator in engine components [1]. However, the full potential of these materials has been limited by low toughness and thermal shock resistance for alumina, and low mechanical strength and poor high-temperature stability below 1280 °C for AT. In view of these limitations, considerable effort has been directed towards improving the mechanical properties and thermal stability of AT through (a) addition of stabilizers [2–4] (e.g. SiO_2, Fe_2O_3 and MgO), (b) incorporation of second phases [5–9] such as mullite and zirconia, (c) reaction sintering of [10] $Al_2O_3/TiO_2/ZrSiO_4$ and $Al_2O_3/TiO_2/ZrSiO_4/MgO$ and (d) grain refinement [11]. Similarly, much attention has been focused on improving the fracture resistance of alumina via microstructural design of duplex [12] or duplex–bimodal [13], heterogeneous [14–16] and layer structures [17–19].

Here we consider a new approach, in which microstructural elements are tailored to provide graded compositions and to generate different modes of strengthening and toughening. The basic idea is to produce a graded dispersion of AT within the alumina–zirconia (AZ) matrix through an infiltration process to yield a layer of homogeneous AZ for hardess and wear resistance, and a tough layer of heterogeneously graded AT/AZ for damage dispersion. This concept is different from various ceramic layer structures which have been developed where alternating homogeneous and heterogeneous layers are laminated to provide a combination of wear and fracture resistance [19–21]. The concept of layered and graded structures with improved mechanical properties has been successfully exploited for mullite/alumina composites by Green and Marple [22–24] and composites of mullite/zirconia-toughened alumina (ZTA), AT/alumina and AT/mullite/ZTA

**Present address*: Physics Department, Faculty of Mathematics and Sciences, Institute of Technology Sepuluh November, Surabaya, Indonesia.
‡To whom correspondence should be addressed.

by Low and co-workers [25–29]. The method involves encasing an alumina or ZTA host body with a graded layer of mullite or AT layer. This was achieved by infiltrating the host body with a silica-rich (e.g. ethyl silicate) or TiO_2-rich (e.g. tetraethyl orthosilicate) solution, followed by firing the composite at an appropriate temperature. Owing to thermal expansion mismatch between mullite or AT and the host body, desirable macroscopic compressive stresses can be induced in the casing. The protective layer inhibits crack growth and thereby improves the effective fracture resistance of the material. A similar infiltration process was used by Tu and Lange [29a] for synthesizing non-oxide ceramics.

In this paper, Part I of the series, we describe details of the synthesis, characterization and physical properties of a layered and graded AT/AZ composite processed through an infiltration method. This method is relatively simple and offers excellent control over the depth of infiltration, which dictates the depth of the graded layer. The presence of the *in-situ* AT phase in the AZ matrix has a profound influence on the graded and physical properties of the composite. The characteristics and properties have been studied using X-ray diffraction (XRD), neutron diffraction, energy-dispersive spectrometry, differential thermal analysis (DTA), thermogravimetric analysis (TGA), thermal dilatometry and scanning electron microscopy (SEM).

2. Experimental procedure

2.1. Processing of samples

A powder mixture of AZ was obtained by wet ball milling 90 wt% α-Al_2O_3 (Al000SG grade Alcoa, USA; of median particle size 0.39 μm) and 10 wt% monoclinic zirconia (m-ZrO_2) (SF Ultra Z-Tech, Australia; of median particle size 0.40 μm). The slurry was then dried and sieved until free flowing (45 μm grid size). The powder mixture was uniaxially pressed in a metal die at a pressure of 37 MPa to yield a bar sample with dimensions of 5 mm × 12 mm × 60 mm. Partial sintering at 1000 °C for 2 h was used to increase the strength of the green body while retaining sufficient porosity (approximately 46%) prior to infiltration.

The porous preforms were initially placed in a vacuum vessel (10^{-3} Torr) before being completely immersed for 24 h in a solution containing 30 wt% $TiCl_4$ (BDH Limited, Poole, England). The infiltrated preforms were then dried at room temperature for 24 h before being heat-treated in a high-temperature furnace (Ceramic Engineering model HT 04/17) at a rate of 1 °C min^{-1} to 450 °C for 30 min, followed by 5 °C min^{-1} to 1550 °C for 3 h, and then furnace-cooled at a rate of 10 °C min^{-1}. For comparison purposes, a control sample of AZ (90:10 alumina: zirconia by weight) was also prepared and heat-treated in the same manner but without being immersed in the solution.

2.2. X-Ray diffraction and high temperature neutron diffraction

The general phase identification and depth profiling of phases formed in the graded sample were done using XRD. XRD patterns of the sintered specimen at various depths (0–1.5 mm) were collected using a Siemens D500 X-ray diffractometer (Cu K_α tube) at 40 kV and 30 mA. An incident beam divergence of 0.3° was used. These patterns were recorded from 17° to 100° in 2θ at a step size of 0.04°, and with a counting time of 2 s per step. The subsurface measurements were made after gradual polishing with emery paper to the required depth.

Rietveld pattern-fitting was employed with the collected patterns to estimate the phase composition. Refinements were made with the LHPM program [30]. The refined parameters were the background profile parameters and 2θ-scale offset as global parameters, and for each phase the scale factor, lattice parameters, preferred orientation factor and pseudo-Voigt peak profile parameters. The crystal structure models used for the refinements have been described in [31].

The weight fraction of phase i at each depth was determined by the external standard approach [32]

$$W_i = \frac{s_i(ZMV)_i\mu^*}{s_s(ZMV)_s\mu_s} \quad (1)$$

where s_i and s_s denote the Rietveld scale factors of sample i and the external standard (i.e. high-purity α-alumina) respectively. Z_i is the number of formula units of phase i (calculated from the refined lattice parameters) with mass M_i in the unit-cell volume V_i. The mass attenuation coefficient (MAC), μ_s, of the standard was calculated whereas the MAC, μ^*, of the specimens was determined by Compton scattering measurements. Details of the experimental procedure used in determining the MAC of the graded material have been reported elsewhere [31, 32].

High-temperature neutron diffraction (HTND) was used to monitor the evolution of phase transformations with the as-fired graded sample at various temperatures (25–1000 °C). This experiment was conducted in order to explain the anomalous thermal expansion behaviour of the graded material at temperatures in the range 700–900 °C (see Fig. 7). The HTND data collection was performed using the medium-resolution powder diffractometer located at the Australian Nuclear Science and Technology Organisation in Lucas Heights, New South Wales. The operating conditions were as follows: $\lambda = 1.664$ A°; 2θ range, 5–138°; step size, 0.1°; counting time, about 40–50 s per step; monochromator of 8 Ge crystals ((115) reflection); 24 ^{3}He detectors 4° apart.

2.3. Microstructural observation

A graded sample was prepared for microstructural study following the standard ceramographic procedure, i.e. polishing to 1 μm finish. The sample was thermally etched at 1500 °C for 10 min to reveal grain boundaries. Micrographs were taken with a JEOL 35C electron microscope operated at 25kV and 0.1μA. The micrographs of the graded material were taken near the edge region, at depths of approximately 300, 600 and 1000 μm. Grain size measurement was conducted by the lineal intercept method [33].

Energy-dispersive X-ray analysis was used to qualitatively display the graded profile in the functionally-graded material (FGM) sample. A sample of 3.5 mm × 6.0 mm × 1.5 mm was obtained by cross-sectionally cutting the as-fired sample. Titanium X-ray mapping of the sample was obtained after the sample had been carbon coated.

2.4. Properties characterization

The bulk density and apparent porosity of the sintered samples were measured following the Australian Standard AS 1774.5 [34]. The percentage reduction in volume was used to determine the shrinkage values.

A Stanton Redcroft STA-780 thermal analyser was used to study the evolution of thermochemical reactions during the heat treatment of samples in air from room temperature to 1400 °C at a heating rate of 10 °C min^{-1} with alumina powder as the reference standard.

The thermal expansion behaviour of sintered samples in air from room temperature to 1300 °C was characterized using a TMA Rigaku Thermoflex 8140 thermoanalyser. Sintered alumina was used as the reference standard, and the heating and cooling rates were 3 °C min^{-1} and 10 °C min^{-1}, respectively. The dimensions of the bar samples for thermal expansion measurement were 20 mm × 3 mm × 3 mm. Depth profiling of the thermal expansion coefficient (TEC) was evaluated by gradually polishing away the sample surface.

The effect of graded structure and ZrO_2 on the short-term thermal stability of the AT phase at 1050 °C was also investigated. XRD patterns were collected from sintered samples which had been annealed at 1050 °C for up to 6 h in order to study the thermal decomposition of AT. The rate of decomposition was determined using integrated intensity ratios of AT to alumina and of rutile to alumina. The α-alumina (0 2 4), AT (0 2 3) and rutile (1 1 0) peaks were selected for the study.

3. Results and Discussion

3.1. Physical character and phase distribution

Table I shows the mass change, bulk density, apparent porosity and shrinkage of the as-fired, infiltrated and uninfiltrated AZ composites. Assuming that all TiO_2 completely reacted with alumina in the matrix to form AT and that 3 wt% tetragonal zirconia (t-ZrO_2) was present (Table II), this mass increase can be related to the presence of as much as 9.2 wt% or 10.0 vol% AT in the bulk. However, the concentration of AT is not uniformly distributed throughout the sample. As shown by the quantitative Rietveld analysis, the content of AT varies from 44.5 wt% on the surface to 5.3 wt% at a depth of 1.5 mm towards the core (see Table II).

The formation of *in-situ* AT (Al_2TiO_5) in the sample is believed to occur via an endothermic sintering reaction between Al_2O_3 and the infiltrated TiO_2 at approximately 1280 °C [35]

$$\alpha - Al_2O_3 + TiO_2\ (\text{rutile}) \rightarrow \beta - Al_2TiO_5 \quad (2)$$

TABLE I Mass changes, densities, porosities and shrinkages of the infiltrated and uninfiltrated (control) specimens: ΔM_a, relative mass difference after and before infiltration; ΔM_b, relative mass difference after drying and before infiltration; ΔM_c, relative mass difference after sintering and before infiltration; D, density; P, porosity; subscripts i and f indicate initial (before infiltration) and final (after sintering), respectively; S, volume shrinkage; values in parentheses are the estimated standard deviation to the left

Specimen	ΔM_b (%)	ΔM_c (%)	D_i ($g\,cm^{-3}$)	D_f ($g\,cm^{-3}$)	P_f (%)	S (%)
Infiltrated	5.4(4)	4.2(6)	2.3(1)	4.07(2)	3.3(3)	40.1(25)
Control	0.2(2)	0.6(5)	2.3(1)	4.06(3)	2.1(4)	46.5(14)

TABLE II Absolute weight fractions of phases in the functionally graded AT/AZ composite at various depths and the AZ ceramic control sample (the values in parentheses are the estimated standard deviation to the left)

Depth (mm)	Weight fraction (%) for the following phases				
	Al_2O_3	AT	m-ZrO_2	t-ZrO_2	Amorphous
0.0	44.4(12)	44.5(15)	5.3(3)	1.0(1)	5(2)
0.1	56.4(15)	34.6(12)	5.8(2)	0.7(1)	2(2)
0.3	80.2(19)	9.5(6)	7.0(2)	1.2(1)	2(2)
0.4	78.9(20)	8.3(6)	7.0(2)	1.0(1)	5(2)
0.8	81.0(20)	7.2(6)	6.8(2)	1.1(1)	4(2)
1.2	84.1(16)	7.7(9)	6.5(2)	2.4(1)	0(2)
1.5	85.7(17)	5.3(9)	6.7(2)	2.1(1)	0(2)
Control	90.3(18)	—	4.0(2)	5.0(1)	1(1)

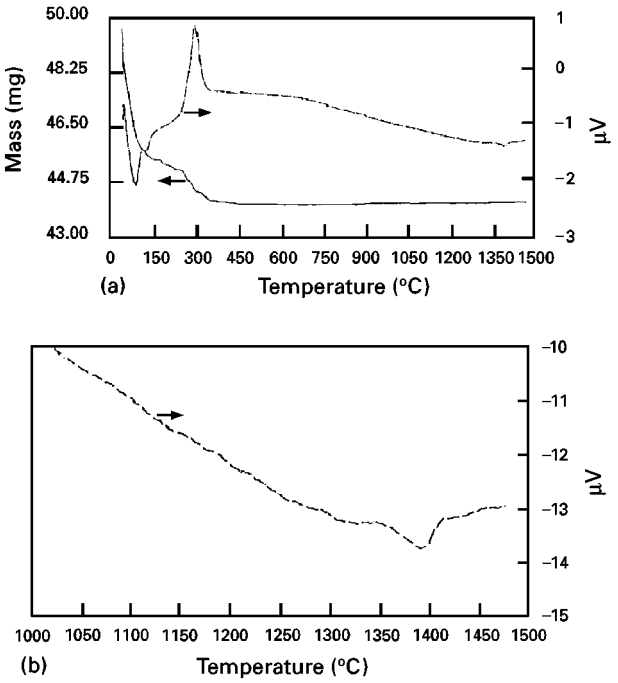

Figure 1 (a) DTA and TGA curves for an AZ preform infiltrated with $TiCl_4$. (b) An enlarged view of the DTA at 1000–1500 °C is also given.

The thermochemical reactions during the firing of an infiltrated sample from room temperature to 1400 °C is depicted in Fig. 1. The first endotherm, centred at 100 °C, is attributed to the removal of physically absorbed water. The exotherm at 300 °C may be related to the decomposition of residual organic matter. The formation of crystalline AT is revealed by an

endothermic enthalpy effect at 1380 °C which is approximately 40 °C higher than that observed for pure AT [36–38] and graded AT/alumina [28]. This higher temperature of AT formation may be attributed to the existence of limited solid solution between ZrO_2 and AT [39]. The display of a negative reaction enthalpy suggests the importance of entropy in the formation of AT, i.e. $-T\,\Delta S$ exceeds $+\Delta H$ to give a negative ΔG. It appears that a random distribution of the Al and Ti atoms on the sites of the pseudobrookite structure [36] is crucial for the stabilization and formation of AT.

Table I shows that the apparent porosity of the infiltrated sample is 3.3% whereas that of the uninfiltrated control sample is 2.1%. A higher sintering temperature (above 1600 °C) or hot pressing may be necessary to achieve nearly full densification. The graded material produced here has a much higher final density when compared with other non-graded AT composites [11, 40, 41], where at least 12% apparent porosity was observed. The volume shrinkages of the infiltrated and uninfiltrated samples are 40.1 and 46.5%, respectively, after sintering. The lower shrinkage of the infiltrated sample can be attributed to the presence of AT, which expands by 11% during its formation, and this hinders sintering or shrinkage.

Qualitative analysis of the XRD data shows that the phases present in the material were AT, α-alumina, m-ZrO_2 and t-ZrO_2. These phases were observed at all sample depths. The absolute weight fractions of phases in the FGM at various depths are presented in Table II. The gradual decrease in absolute weight fraction of AT with increasing depth shows that the material exhibits a graded compositional character. The depth profile of alumina content increases complementarily with that of AT.

The average content of t-ZrO_2 in the graded sample was less than that in the AZ control sample. It is interesting to note that this content increased slightly with increasing depth. As proposed by Wohlfromm *et al.* [42], the "weak" AT matrix was responsible for the inability to retain the t-ZrO_2 phase at room temperature. Since the amount of AT decreases with increasing depth, it follows that the ability of the graded material to retain t-ZrO_2 should be higher in the core than near the surface. It appears that the presence of AT has induced residual tensile stresses near the surface which may be responsible for enhancing the tetragonal → monoclinic phase transformation. The microstructural study (see Fig. 4) confirms the results of phase analysis in that no zirconia grains were embedded within alumina grains at the near-surface region, a characteristic associated with m-ZrO_2 particles [43]. By contrast, fine t-ZrO_2 particles were embedded in alumina grains near the inner region.

The amorphous phase content at various depths was determined by subtracting the total crystalline phases content from unity. Approximately 3 wt% amorphous material was found in the graded material. The value of amorphous phase MAC ($Cu\,K_\alpha$) at each depth is between 69.8 and 125.8 $cm^2\,g^{-1}$ [32]. This value indicates that the phase is either amorphous AT [36] or amorphous TiO_2 (MAC ($Cu\,K_\alpha$) = 127.25 $cm\,g^{-1}$), which has experienced incomplete crystallization to form rutile.

Qualitative energy-dispersive X-ray microanalysis was used to verify the graded compositional character of a finely polished graded sample. The X-ray emission

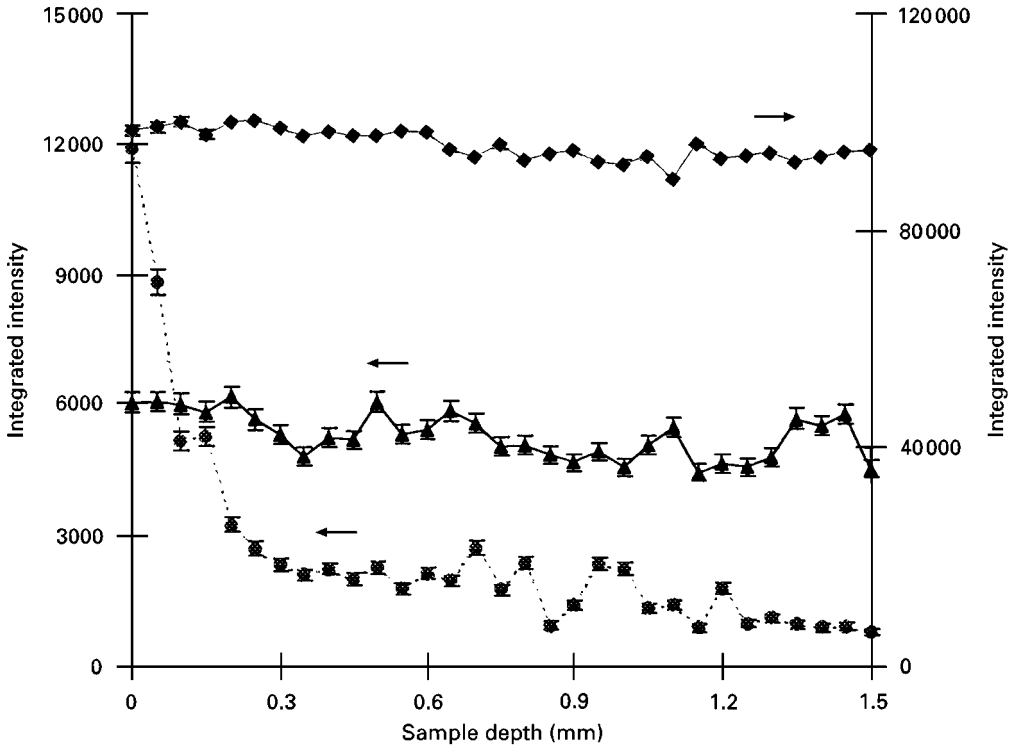

Figure 2 X-ray characteristic emissions of Ti K_α (- - -●- - -), Al K_α (—◆—) and Zr L_α (—▲—) with depth of FGM sample measured using energy-dispersive X-ray microanalysis. Error bars indicate 2 × estimated standard deviations.

intensities of Ti K_α, Al K_α and Zr L_α were collected from the (near) surface to the centre with both a spot size and a step size of 50 μm. Fig. 2 shows the plot of the X-ray emission integrated intensities of the lines versus sample depth. It is clearly shown that titanium emissions reduce with increasing depth whereas those of aluminium and zirconium are nearly constant. This observation suggests that infiltration has led to the formation of a graded microstructure. Similar graded profiles have been obtained for the infiltration processed mullte/alumina system [22]. Therefore, these results complement those of XRD quantitative phase analysis.

Fig. 3a shows the Ti dot map for the region near the surface (0–500 μm) of the graded material. The back-scattered scanning electron micrograph of the associated region is shown in Fig. 3b. A gradual decrease in Ti (or AT) content with increasing depth is clearly evident. A similar depth profile character has also been observed by Low and co-workers [28, 29] for infiltration-processed AT/alumina and AT/mullite/ZTA composites. This observation serves to verify the graded compositional character of the material.

3.2. Microstructure

Micrographs of the infiltrated sample are shown in Fig. 4. The alumina grains exhibit a dark color and AT grains are slightly lighter or grey coloured. The bright grains are zirconia. At 20 μm depth, many grey grains are observed. The number of these grains reduces with increasing depth, which indicates that the surface of the as-fired infiltrated specimen is AT rich and that its content reduces with an increase in depth.

Fig. 5 shows the results of alumina grain size measurement using a lineal intercept method. The average grain size of alumina tends to increase with increasing depth. The grain growth of alumina is clearly controlled by the presence of both AT and m-ZrO_2, the content of which reduces with increasing sample depth, presumably through a pinning mechanism [13, 44, 45]. Additions of ZrO_2 [46] and mullite

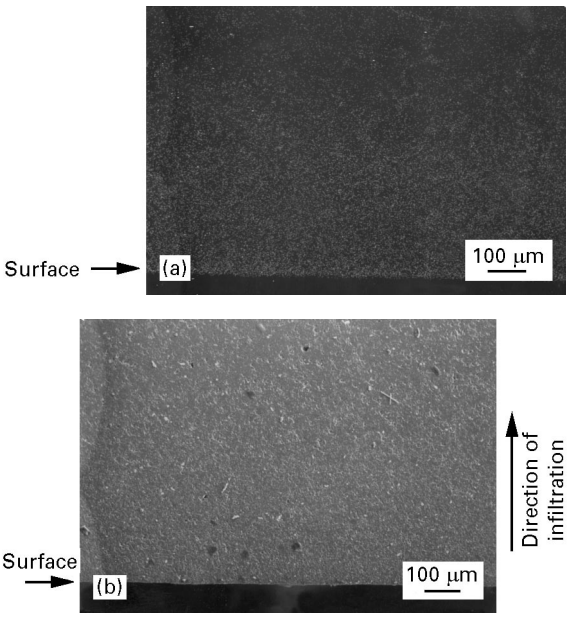

Figure 3 (a) Ti dot map at region of approximately 0–500 μm within the AT/AZ FGM. (b) Back-scattered scanning electron micrograph of the associated region. Note the same size of the indicator bars.

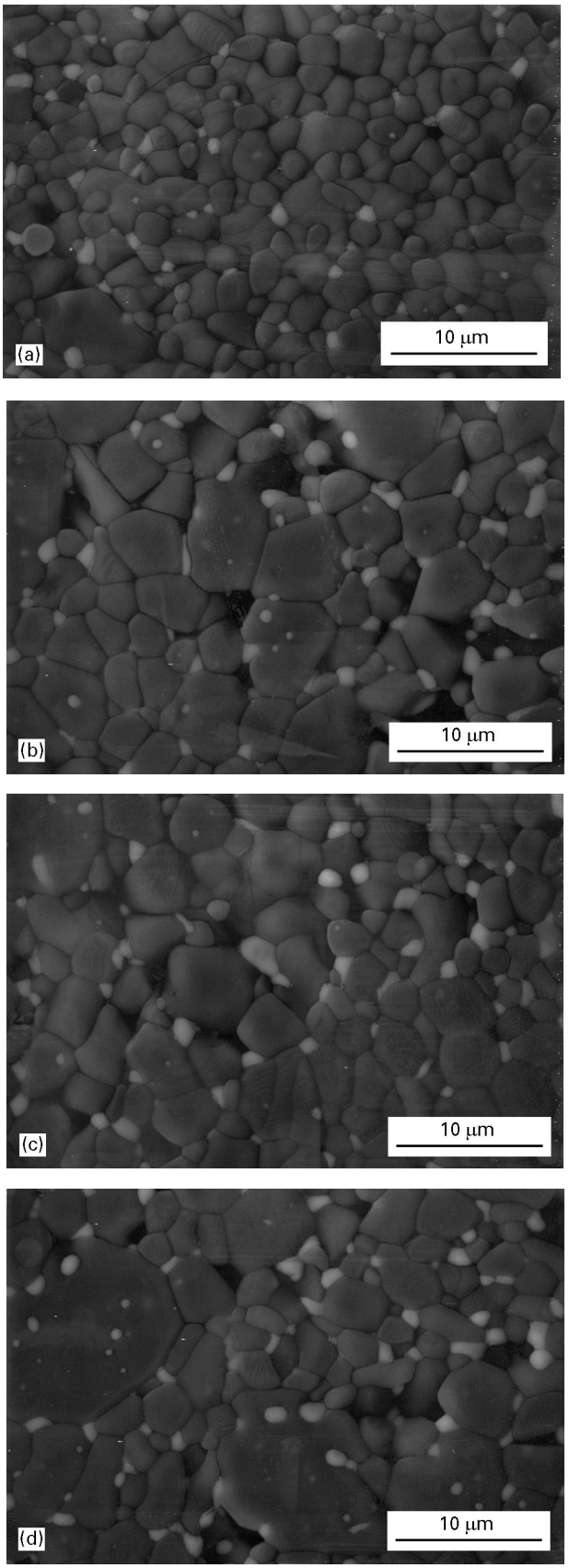

Figure 4 Microstructure of the as-fired infiltrated specimen at depth of (a) 0.02 mm (near the surface), (b) 0.3 mm, (c) 0.6 mm and (d) 1.0 mm. The dark grains are alumina, the grey grains are AT, and the light grains are zirconia. The sample was polished and then thermally etched at 1500 °C for 10 min.

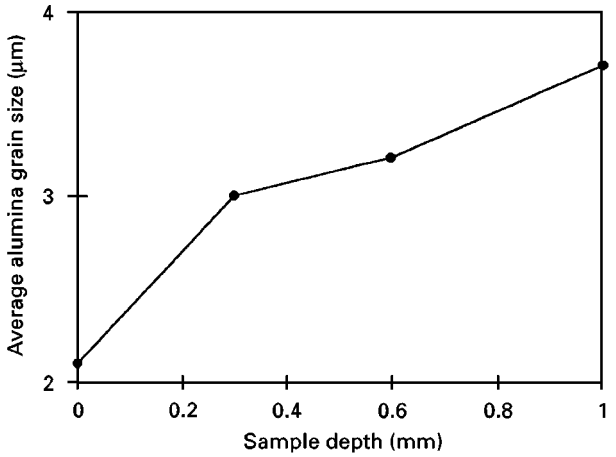

Figure 5 Average α-alumina grain size at various depths of the functionally graded AT/AZ composite.

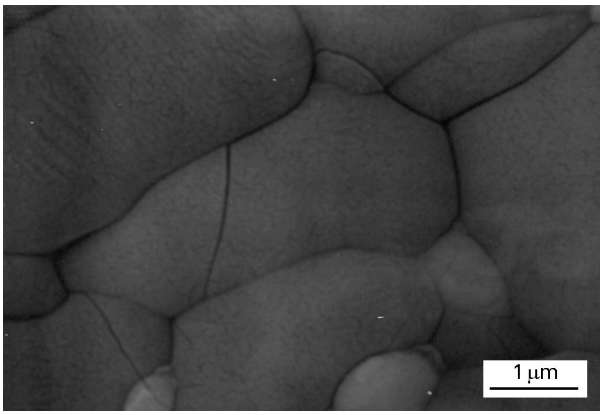

Figure 6 Microcracking phenomena in AT and zirconia grains of AT/AZ FGM.

TABLE III TEC values of the AT/AZ FGM and AZ control sample between 20 and 1300 °C

Specimen	Average TEC ($10^{-6}\,°C^{-1}$)
FGM, unpolished, between 20 and 750 °C	5.9
FGM, unpolished, between 800 and 1300 °C	5.0
FGM, unpolished, between 20 and 1300 °C	5.6
FGM, 0.3 mm polished	7.3
FGM, 0.5 mm polished	7.4
Control sample (non-FGM)	7.4

[47] have been observed to be effective in controlling the abnormal grain growth of alumina.

There are other features which can be discerned from the microstructural observation of the graded material. Firstly, the "porous" polished surface can be attributed to profused grain pull-outs during polishing by virtue of a large thermal expansion mismatch between alumina and AT [42, 44, 48]. Secondly, intragranular microcracks prevail in AT grains (Fig. 6) as a result of pronounced anisotropy in thermal expansion [49]. This type of microcracking is well distributed within the near-surface region and occurs usually along the short axis, normal to the directions of high expansion caused by the development of tensile stresses [50]. It is worth noting that these intragranular microcracks generally occur in AT grains which are larger than 2 μm. This suggests that there is a critical grain size for spontaneous microcracking in AT grains [42, 49]. The AT grains prefer to grow along the long axis rather than the short axis, causing tensile stresses to be induced along this axis which result in the break-up of the grains. Thirdly, intragranular microcracking also occurs in zirconia grains (see Fig. 6). Such microcracks tend to occur along the short axis and are surrounded by AT grains. It is also worth noting that no microcracks were observed in alumina-surrounded zirconia grains. The microcracking in the zirconia grains is driven by the intragranular microcracks in AT grains. Intragranular cracking of m-ZrO_2 grains has been commonly observed in zirconia-toughened alumina ceramics [43, 51]. Finally, it is worth emphasizing that the infiltration process offers a simple but elegant approach that can be utilized to engineer ceramics with graded composition and microstructure for both functional and structural applications.

3.3. Thermal expansion characteristics

TEC values of the graded material at various polishing depths and the control sample are shown in Table III. The average value of TEC of the graded material increases with increasing depth, i.e. from $5.6 \times 10^{-6}\,°C^{-1}$ on the surface to $7.4 \times 10^{-6}\,°C^{-1}$ at 0.5 mm depth. This increase is associated with the gradual removal of the low-thermal expansion AT phase from the surface of the material. By polishing up to 0.5 mm depth, the TEC value of graded material has approached that of the control sample, i.e. $7.4 \times 10^{-6}\,°C^{-1}$. The presence of a low-thermal-expansion surface layer may impart improved thermal shock resistance to the material.

It is interesting to note that the as-fired graded material exhibits an anomalous thermal expansion curve between 750 and 850 °C (Fig. 7a). The TEC drops from $5.5 \times 10^{-6}\,°C^{-1}$ at 750 °C to $4.5 \times 10^{-6}\,°C^{-1}$ at 850 °C. In order to explain the phenomenon responsible for this thermal expansion "kink", HTND measurements were performed at various temperatures (Fig. 8). As can be seen from the Figure, the m-ZrO_2 peaks (denoted as Z-m) reduce significantly with increasing temperature. This trend is accompanied by increases in the t-ZrO_2 peak intensities (denoted as Z-t). This type of transformation is followed by a reduction in unit cell volume by 4% [51]. Thus, this observation confirms that the anomalous thermal expansion behaviour of the FGM was due to the m-ZrO_2 → t-ZrO_2 transformation. It is also possible that crack healing in AT grains [52] may cause a reduction in grain dimensions and thus a drop in the thermal expansion of the material. This crack healing is believed to commence at approximately 750 °C (see Fig. 7b), which corresponds to the start of decline in the thermal expansion curve. This phenomenon together with the m-ZrO_2 → t-ZrO_2 transformation is believed to be responsible for the observed sharp drop in thermal expansion values of the graded material at elevated temperatures.

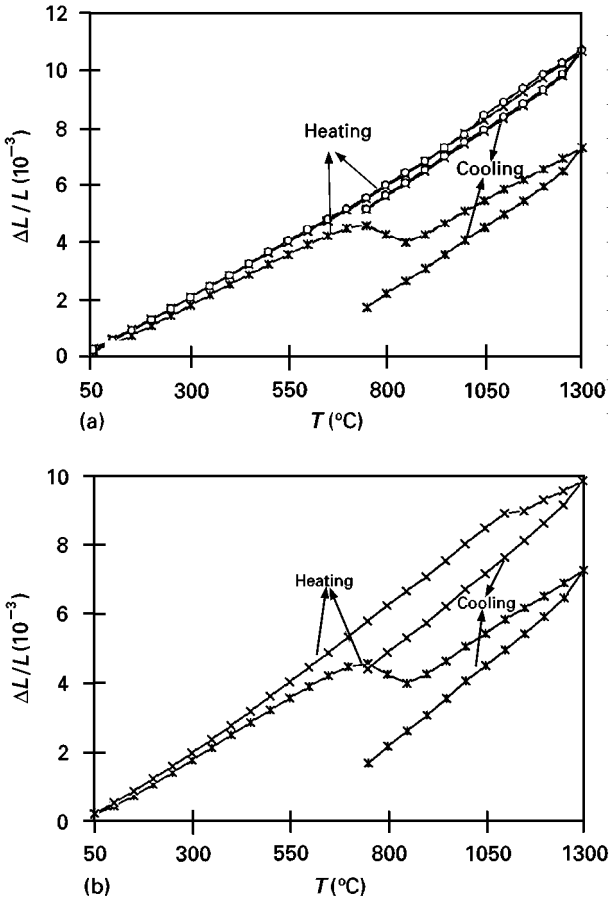

Figure 7 Thermal expansion behaviour of AT/AZ FGM and AZ control sample between 20 and 1300 °C: (a) FGM as-fired (—∗—) and after polishing up to 0.3 mm (—×—) and 0.5 mm (—○—) depths; (b) the as-fired FGM (—∗—) and AZ control (—×—) samples.

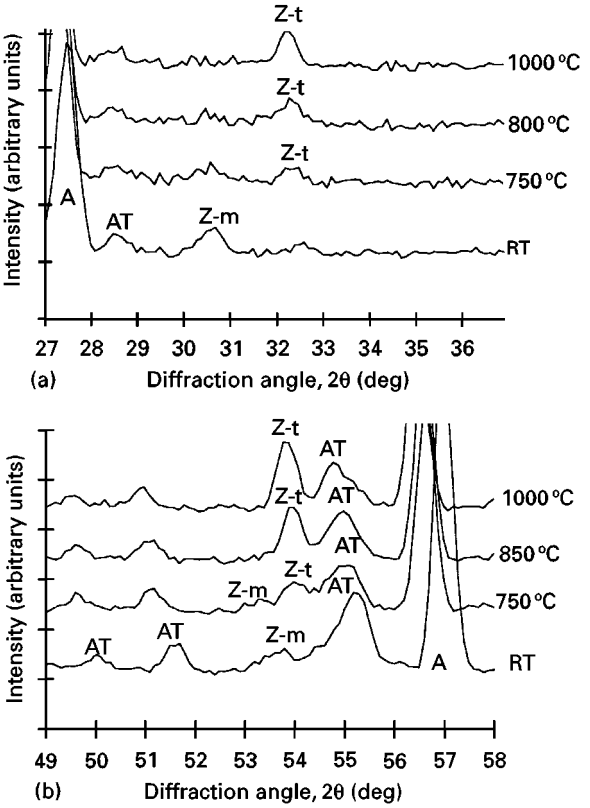

Figure 8 Neutron diffraction patterns of the AT/AZ FGM collected at room temperature (RT) and elevated temperatures ($\lambda = 1.664$ Å). Patterns are highlighted in the 2θ range of (a) 27–37° and (b) 49–59°. AT, aluminium titanate; A, α-alumina; Z-m, m-ZrO_2; Z-t, t-ZrO_2.

Another anomalous behaviour in thermal expansion is also observed in the control sample at approximately 1100 °C (see Fig. 7b), where the TEC value drops by approximately $0.2 \times 10^{-6}\,°C^{-1}$. This decrease is well established to arise from the m-ZrO_2 → t-ZrO_2 transformation [51]. Such a drop was not observed at 1100 °C in the graded material because all m-ZrO_2 had already been transformed into the tetragonal structure at a lower temperature, i.e. 750 °C. The drop in the value of the TEC is greater in the graded sample than in the control since the former has more m-ZrO_2 at room temperature than that of the latter, as previously described in Section 3.1. The presence of AT appears to have a profound influence on the transformation temperature of m-ZrO_2 to t-ZrO_2, which may also be ascribed to the existence of a solid solution between AT and ZrO_2.

3.4. Thermal stability of aluminium titanate/alumina–zirconia material

One of the limitations of AT is its thermal decomposition of the material into parent phases, i.e. α-alumina and rutile, between 900 and 1100 °C [35]. Extensive studies have been conducted by various workers to understand the mechanism of decomposition and to stabilize the material by incorporating second phases such as ZrO_2 [4], SiO_2 [4], MgO [3, 4, 53] and Fe_2O_3 [2, 3]. It has been shown by these researchers that MgO and Fe_2O_3 are the most effective materials for stabilizing the material, whereas ZrO_2 and SiO_2 are less effective.

Fig. 9 shows the XRD patterns from the surface of the graded material after annealing at 1050 °C for 0, 2, 4 and 6 h. Note that, from the compositional analysis described earlier, the surface of FGM contained 44.5 wt% AT, 44.4 wt% α-alumina and 6.3 wt% zirconia. It is evident from the figure that the AT on the surface of grade material has decomposed into α-alumina and rutile. This phenomenon is particularly evident from the increase in the intensity of the rutile (1 0 1) peak with prolonged annealing time.

Fig. 10 shows the results of thermal decomposition of FGM at various annealing times. Results from a study of Hwang *et al.* [48] on the thermal decomposition of AT-dispersed alumina are also presented for comparison. It is clear that the AT-to-alumina peak ratio in the graded material decreases slowly with increase in annealing time, while the rutile-to-alumina peak ratio increases with increasing annealing time. By contrast, the AT-to-alumina peak ratio in the AT-dispersed alumina decreases rapidly, and the rutile-to-alumina peak ratio increases abruptly with increasing annealing time, indicating a high degree of thermal decomposition.

These results indicate that the presence of zirconia has apparently affected the decomposition of AT in a positive way. Fig. 10 also shows that the thermal decomposition rate of graded material is clearly much

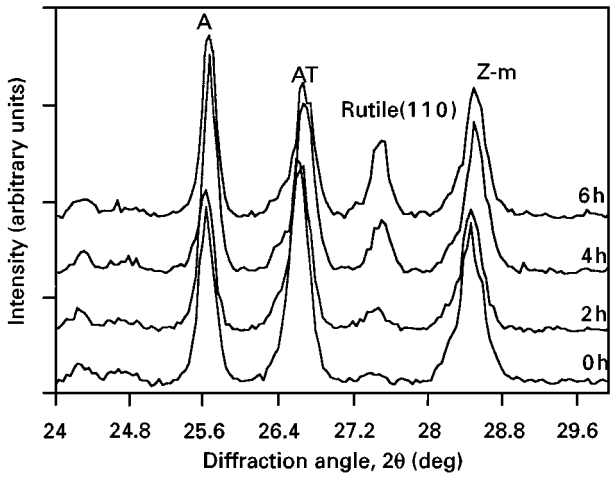

Figure 9 XRD patterns (Cu K_α radiation) from the surface of the FGM for decomposition study after annealing at 1050 °C for 0, 2, 4 and 6 h. Note in particular the peak increase in rutile (1 1 0). AT, aluminium titanate; A, α-alumina; Z-m, m-ZrO_2.

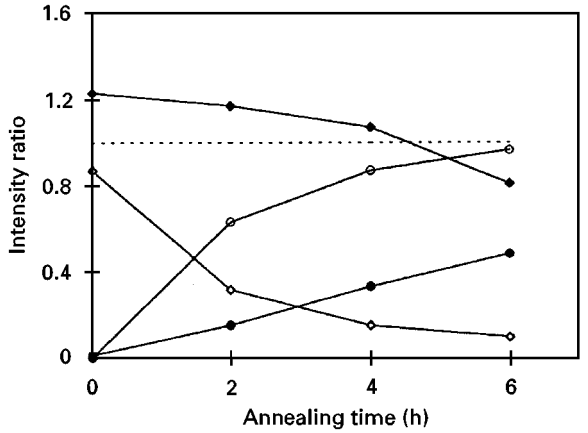

Figure 10 The decomposition rate of AT in the layered and graded AT/AZ material for the integrated line intensity ratios of AT (0 2 3) to alumina (0 2 4) (—◆—) and of rutile (1 1 0) to alumina (0 2 4) (—●—). The decomposition rate of a non-graded AT/alumina control material for the integrated line intensity ratios of AT (0 2 3) to alumina (0 2 4) (—◇—) and of rutile (1 1 0) to alumina (0 2 4) (—○—) [48] is also presented for comparison. (- - - - - -), complete decomposition level where the ratio of rutile to alumina is unity.

less than that of the AT-dispersed alumina system [48]. While AT in the latter decomposed rapidly with increasing annealing time, the former was reasonably stable for short-term annealing times (less than 6 h). However, it is believed that the thermal stability of graded material will eventually degrade with longer annealing times because ZrO_2 is not a good stabilizer for AT [4]. As proposed by Wohlfromm *et al.* [42], the negligible effect of zirconia in the stabilization of AT may be attributed to the inability of relatively large Zr^{4+} (ionic radius, 0.79 Å) to substitute for the smaller Ti^{4+} (0.68 Å) or Al^{3+} (0.51 Å) in AT. Oxygen deficiency [6] in the AT structure may also reduce its ability to be stabilized by zirconia. On the contrary, MgO and Fe_2O_3 are excellent stabilizers of AT [2, 3].

4. Conclusions

AT/AZ with graded properties has been synthesized using an infiltration process. The presence of the *in-situ* AT phase in the AZ matrix has a profound influence on the physical properties of the composite. The infiltration approach offers an elegant means of tailoring the composition and microstructure of graded materials. The characteristics and properties have been studied using XRD, neutron diffraction, DTA, TGA, thermal dilatometry and scanning electron microscopy.

XRD and energy-dispersive X-ray microanalysis have verified the graded compositional character of the material. The presence of microcracking in AT grains and the growth control of alumina grains by both AT and ZrO_2 have been revealed by SEM.

The graded material displays continuous changes in thermal expansion values. The near-surface region has a TEC value of $5.9 \times 10^{-6}\,°C^{-1}$ compared with $7.4 \times 10^{-6}\,°C^{-1}$ at the core. This graded property is due to the presence of AT, the amount of which is gradually reduced from the surface to the core. The presence of ZrO_2 has a favourable effect on the stabilization and prevention of AT against thermal decomposition.

Acknowledgements

S. Pratapa is very grateful to the Australian Agency for International Development for providing a scholarship. I. Low is grateful to the Australian Research Council and the Australian Institute of Nuclear Science and Engineering (AINSE) for financial support (AINSE Grant 96/142). Dr B. Hunter and Mr R. Skala assisted with the collection of HTND data. We thank Ms E. Miller for assistance with SEM. We are grateful to Professor K. Niihara of Osaka University, Japan, for providing facilities to perform the thermal expansion experiments.

References

1. P. STINGL, J. HEINRICH and J. HUBER, in Proceedings of the Second International Symposium on Ceramic Materials and Components for Engines, Lubeck-Travemunde, April 1986, edited by W. Bunk and H. Hausner (DKG, Bad Honnef, 1986) pp. 369–380.
2. G. TILLOCA, *J. Mater. Sci.* **26** (1991) 2809.
3. G. BATTILANA, V. BUSCAGLIA, P. NANNI and G. ALIPRANDI, in "High performance materials in engine technology", edited by P. Vincenzini (Techna Srl., 1995) pp. 147–154.
4. M. ISHITSUKA, T. SATO, T. ENDO and M. SHIMADA, *J. Amer. Ceram. Soc.* **70** (1987) 69.
5. H. MORISHIMA, Z. KATO and K. UEMATSU, *ibid.* **69** (1986) C226.
6. P. PENA, S. DE AZA and J. S. MOYA, in Ceramic Microstructures '86. Role of Interfaces, edited by J. Pask and A. G. Evans (Plenum, New York, 1987) pp. 847–857.
7. H. MORISHIMA, *J. Mater. Sci. Lett.* **6** (1987) 389.
8. H. A. THOMAS, R. STEVENS and E. GILBART, *J. Mater. Sci.* **26** (1991) 3613.
9. F. J. PARKER, *J. Amer. Ceram. Soc.* **73** (1990) 929.
10. H. WOHLFROMM, J. S. MOYA and P. PENA, *J. Mater. Sci.* **25** (1990) 3753.
11. B. FREUDENBERG and A. MOCELLIN, *J. Amer. Ceram. Soc.* **70** (1987) 33.
12. M. P. HARMER, H. M. CHAN and G. A. MILLER, *ibid.* **75** (1992) 1715.
13. N. P. PADTURE, S. J. BENNISON and H. M. CHAN, *ibid.* **76** (1993) 2312.

14. L. AN and H. M. CHAN, *J. Amer. Ceram. Soc.* **79** (1998) 3142.
15. P. L. CHEN and I. W. CHEN, *J. Amer Ceram. Soc.* **75** (1992) 2610.
16. J. WANG, C. B. PONTON and P. M. MARQUIS, *Brit. Ceram. Trans.* **92** (1993) 67.
17. P. E. D. MORGAN and D. B. MARSHALL, *J. Amer. Ceram. Soc.* **78** (1995) 1553.
18. C. J. RUSSO, M. P. HARMER, H. M. CHAN and G. A. MILLER, *ibid.* **75** (1992) 3396.
19. L. AN, H. M. CHAN, N. P. PADTURE and B. R. LAWN, *J. Mater. Res.* **11** (1996) 204.
20. N. P. PADTURE, D. C. PENDER, S. WUTTIPHAN and B. R. LAWN, *J. Amer. Ceram. Soc.* **78** (1995) 3160.
21. H. LIU, B. R. LAWN and S. M. HSU, *ibid.* **79** (1996) 1009.
22. B. R. MARPLE and D. J. GREEN, *ibid.* **73** (1990) 3611.
23. *Idem.*, *ibid.* **74** (1991) 2453.
24. *Idem.*, *ibid.* **75** (1992) 44.
25. I. M. LOW, R. D. SKALA, R. RICHARDS and D. S. PERERA, *J. Mater. Sci. Lett.* **12** (1993) 1585.
26. I. M. LOW, R. D. SKALA and D. S. PERERA, *ibid.* **13** (1994) 1334.
27. I. M. LOW, R. D. SKALA and D. LI, *ibid.* **13** (1994) 1354.
28. I. M. LOW, R. D. SKALA and D. ZHOU, *ibid.* **15** (1996) 345.
29. S. PRATAPA and I. M. LOW, *ibid.* **15** (1996) 800.
29a. W. C. TU and F. F. LANGE, *J. Amer. Ceram. Soc.* **78** (1995) 3277.
30. R. J. HILL, C. J. HOWARD and B. A. HUNTER, "LHPM, Rietveld refinement program manual", (Australian Atomic Energy Commision, Lucas Heights Research Laboratory, Menai, New South Wales, 1986).
31. S. PRATAPA, MSc thesis, Curtin University of Technology, Perth, Western Australia (1997).
32. S. PRATAPA, B. H. O'CONNOR and I. M. LOW, *Powder diffraction* (1998) in press.
33. J. C. WURST and J. A. NELSON, *J. Amer. Ceram. Soc.* **55** (1972) 109.
34. Australian Standards, Refractories and Refractory Materials-Physical Test Methods, Method 5: The Determination of Density, Porosity and Water Absorption: 1774.5, Standard Australia (1989).
35. E. KATO, K. DAIMON and J. TAKAHASHI, *J. Amer. Ceram. Soc.* **63** (1980) 355.
36. A. FELTZ and F. SCHMIDT, *J. Eur. Ceram. Soc.* **6** (1990) 107.
37. G. BAYER, *J. Less-Common Metals* **24** (1971) 129.
38. M. S. GANI and R. MCPHERSON, *Thermochim. Acta* **7** (1973) 251.
39. Y. OHYA, K. HAMANO and Z. NAKAGAWA, *Yogyo-Kyokai-Shi* **91** (1993) 289.
40. M. PERSSON, L. HERMANSSON and R. CARLSSON, *Sci. Ceram.* **11** (1981) 479.
41. D. P. H. HASSELMANN, K. Y. DONALDSON, E. M. ANDERSON and J. A. JOHNSON, *J. Amer. Ceram. Soc.* **76** (1993) 2180.
42. H. WOHLFROMM, T. EPICIER, J. S. MOYA, P. PENA and G. THOMAS, *J. Eur. Ceram. Soc.* **7** (1991) 385.
43. B. LEE and K. HIRAGA, *J. Mater. Res.* **9** (1994) 1199.
44. J. L. RUNYAN and S. J. BENNISON, *J. Eur. Ceram. Soc.* **7** (1991) 93.
45. L. M. BRAUN, S. J. BENNÌSON and B. R. LAWN, *J. Amer Ceram. Soc.* **75** (1992) 3049.
46. F. F. LANGE and M. M. HIRLINGER, *ibid.* **67** (1984) 164.
47. B. R. MARPLE and D. J. GREEN, *J. Mater. Sci.* **28**, (1993) 4637.
48. C. HWANG, Z. NAKAGAWA and K. HAMANO, *J. Ceram. Soc. Jpn.* **102** (1994) 253.
49. J. J. CLEVELAND and R. C. BRADT, *J. Amer. Ceram. Soc.* **61** (1987) 478.
50. E. A. BUSH and F. A. HUMMEL, *ibid.* **42** (1959) 388.
51. J. WANG and R. STEVENS, *J. Mater. Sci.* **24** (1989) 3421.
52. Y. OHYA, Z. NAKAGAWA and K. HAMANO, *J. Amer. Ceram. Soc.* **71** (1988) C232.
53. V. BUSCAGLIA, P. NANNI, G. BATTILANA, G. ALIPRANDI and C. CARRY, *J. Eur. Ceram. Soc.* **13** (1994) 411.

Received 12 August 1997
and accepted 18 March 1998